NIH Public Access
Author Manuscript
Neuron. Author manuscript; available in PMC 2012 May 12.

Published in final edited form as:
Neuron. 2011 May 12; 70(3): 510–521. doi:10.1016/j.neuron.2011.02.057.

Maturation of a Recurrent Excitatory Neocortical Circuit by Experience-Dependent Unsilencing of Newly-Formed Dendritic Spines

Michael C. Ashby[1] and **John T.R. Isaac**[2]
Developmental Synaptic Plasticity Section, National Institute of Neurological Disorders and Stroke, National Institutes of Health, 35 Convent Drive, Bethesda, MD 20892, USA.

SUMMARY

Local recurrent excitatory circuits are ubiquitous in neocortex, yet little is known about their development or architecture. Here we introduce a quantitative technique for efficient single cell resolution circuit mapping using 2-photon (2P) glutamate uncaging and analyze experience-dependent neonatal development of the layer 4 barrel cortex local excitatory circuit. We show that sensory experience specifically drives a 3-fold increase in connectivity at postnatal day (P) 9, producing a highly recurrent network. A profound dendritic spinogenesis occurs concurrent with the connectivity increase, but this is not experience-dependent. However, in experience-deprived cortex, a much greater proportion of spines lack postsynaptic AMPA receptors (AMPARs) and synaptic connectivity via NMDA receptors (NMDARs) is the same as in normally-developing cortex. Thus we describe a new approach for quantitative circuit mapping and show that sensory experience sculpts an intrinsically-developing template network, which is based on NMDAR-only synapses, by driving AMPARs into newly-formed silent spines.

INTRODUCTION

The majority of synaptic inputs onto neurons in the neocortex originate from nearby neurons within the same cortical area, producing local microcircuits that are ubiquitous in neocortex (Braitenberg and Schüz, 1998; Douglas and Martin, 2004; White, 2007). Local excitatory connections provide the major excitatory input to neocortical principal neurons, are highly recurrent and are critically important for information processing, particularly in sensory neocortex (Douglas et al., 1995; Buonomano and Maass, 2009; Rigas and Castro-Alamancos, 2009). Despite the ubiquitous nature of local excitatory circuits very little is known about their organization and almost nothing known about development at the level of connections between individual neurons, thus leading to a poor understanding of mature network architecture.

Correspondence should be addressed to M.C.A. (M.C.Ashby@bristol.ac.uk) or J.T.R.I. (isaac_john@lilly.com).
[1]Present address: School of Physiology and Pharmacology, University of Bristol, Medical Sciences Building, University Walk, Bristol, BS8 1TD, UK.
[2]Present address: Lilly UK, Erl Wood Manor, Windlesham, Surrey, GU20 6PH, UK.

Publisher's Disclaimer: This is a PDF file of an unedited manuscript that has been accepted for publication. As a service to our customers we are providing this early version of the manuscript. The manuscript will undergo copyediting, typesetting, and review of the resulting proof before it is published in its final citable form. Please note that during the production process errors may be discovered which could affect the content, and all legal disclaimers that apply to the journal pertain.

SUPPLEMENTAL DATA

Supplemental data including Supplemental Introduction, Supplemental Experimental Procedures, eight Supplemental Figures and one Supplemental Table can be found accompanying.

NIH-PA Author Manuscript
NIH-PA Author Manuscript
NIH-PA Author Manuscript

NIH-PA Author Manuscript

NIH-PA Author Manuscript

NIH-PA Author Manuscript

Layer 4 of the rodent barrel cortex is the primary input layer for ascending sensory information arriving via thalamocortical fibers (Petersen, 2003). Layer 4 contains clusters of neurons, named barrels, each of which receives topographically-mapped input from a corresponding whisker; this provides an anatomical correlate for whisker receptive fields. Cortical processing of ascending sensory information is thought to begin in layer 4, with the recurrent excitatory network of stellate cells a critical component of this first processing step (Douglas et al., 1995; Bruno and Sakmann, 2006). During early postnatal development, receptive fields in layer 4 emerge in a process that is driven by whisker experience (Feldman and Brecht, 2005). The rapid development of receptive fields (Stern et al., 2001) and the experience-dependent synaptic plasticity of many cortical pathways also occurs at this time (Bender et al., 2006; Allen et al., 2003; Cheetham et al., 2007). Nevertheless, it is not clear how synaptic and anatomical changes at the critical level of individual connections interact to produce network architecture that is capable of processing sensory information.

To understand the development and organization of local circuits it is necessary to investigate connectivity and the synaptic properties of connections between individual identified neurons in sufficient number to allow a quantitative description of the circuit. Mammalian neocortex is composed of heterogeneous, sparsely-connected neuronal populations. This presents a major obstacle for the analysis of circuit connectivity because of the difficulty of identifying and stimulating individual neurons. Simultaneous electrophysiological recordings have been used to analyze multiple neurons (eg -Thomson et al., 2002), but this is very time-consuming, limiting the practicality of a detailed analysis of circuit development. Optical stimulation methods have been used (Nikolenko et al., 2007; Matsuzaki et al., 2008; Dantzker and Callaway, 2000; Petreanu et al., 2007), but, so far, such approaches have not been shown to be suitable for probing local circuit connections with single cell resolution. This is largely due to relatively low spatial resolution of the excitation illumination profile leading to stimulation of multiple and/or off-target cells.

We now describe the development of a high-resoution 2P glutamate uncaging technique that reliably and selectively activates single, identified neurons in intact tissue. Combined with patch-clamp electrophysiology and 2P imaging of dendritic structure, we used this technique to analyze the developmental and experience-dependent changes in the layer 4 excitatory stellate cell network in barrel cortex.

RESULTS

Photostimulation of single, targeted neurons in intact tissue

For glutamate uncaging to be useful in identifying synaptic connections with single cell resolution, the photostimulation must fulfill six key criteria: (1) repeatable trial-by-trial activation of the targeted neuron, (2) reliable activation of the targeted neuron, (3) single cell spatial resolution of uncaging, (4) specificity of activation to the visually identified targeted neuron and not neighbors or dendrites of passage, (5) unambiguous detection of evoked synaptic events and (6) selective activation of monosynaptic connections.

To determine the parameters by which 2P glutamate uncaging can achieve these requirements, we made whole-cell recordings from neurons in acutely-prepared thalamocortical slices containing barrel cortex from mice aged P4–12 and superfused the slices with MNI-caged glutamate. For uncaging we used a 2P laser beam that under-filled a 40× water immersion lens (NA 0.8) to produce a slightly enlarged point spread function (Figure S1, Supplemental Experimental Procedures). The uncaging beam was targeted to neuronal somata using Dodt gradient contrast images of the slice (Figure 1A).

NIH-PA Author Manuscript

NIH-PA Author Manuscript

NIH-PA Author Manuscript

First we explored a large number of combinations of laser power and duration of illumination (106 cells in which 507 parameter combinations were tested in 2237 trials) to find uncaging parameters set that repeatedly and reliably triggered action potentials in the targeted neuron. We found that short-lasting and intense uncaging did not reliably activate all neurons (data not shown). In contrast, longer (75 ms), less intense photostimulation triggered spiking much more reliably (Figure 1A). Such photostimulation drove spiking in 95 % of cells tested, triggering spikes in 97 % of trials in those cells (Figure S2A). These factors combined produced an average probability of evoking an action potential (Pspike) of 0.93 ±0.02 (mean ± sem, n = 70 cells; number of spikes evoked: mean = 1.81 ±0.05, mode = 1, n = 577 trials; spike frequency when multiple spikes evoked = 35.7 ±12.1 Hz, mean ± SD, n=299 trials; Figures 1B & S2BC). Pspike was not significantly changed by depth, age or cell type (although the total number of spikes evoked did decrease with age and depth, the probability of evoking at least one spike (Pspike) remained unchanged) (Figure S2D–I). Evoked spikes occurred between 15 – 189 ms after onset of photostimulation (earliest spike to 99th percentile; 577 trials from 70 cells; Figure 1C), thus defining the time window over which the photostimulation could evoke postsynaptic responses in other neurons (termed 'detection period'). This latency relationship was unaffected by depth, age and neuronal cell type (Figure S2J–L). Therefore, our photostimulation method fulfils the repeatability and reliability requirements specified in the first two criteria above.

We measured the spatial resolution of uncaging by targeting the laser to locations at varying distances from the soma of recorded cells (Figure 1D). Spiking was only triggered when the laser was targeted to within 3 μm of the edge of the cell soma (Figure 1E, all three dimensions pooled, 215 locations from 15 cells). Moreover, targeting the laser to the center of the soma did not trigger spiking, confirming the small volume of excitation and the benign nature of laser exposure itself. Given the density of somata in layer 4 barrel cortex (Lefort et al., 2009), our photostimulation technique has sufficient spatial resolution to selectively stimulate individual cells and not their neighbors, fulfilling criterion 3.

Uncaging of glutamate preferentially triggers spiking when targeted to perisomatic regions compared to dendrites (Nikolenko et al., 2007; Matsuzaki et al., 2008; Dantzker et al., 2000; Shepherd et al., 2003). However, incorrect identification of a connected presynaptic neuron could arise if 2P photostimulation can also elicit action potentials by activating dendrites from cells with distant somata (criterion 4). When deliberately targeted for uncaging (Fig. 1F), uncaging onto axons never triggered spiking (n = 14 from 6 cells) and when dendrites (including spines) were targeted, the proportion of targets that triggered spiking was low, and those that did trigger spiking did so unreliably (Figures 1B & S2A). Overall, there is a very low probability of evoking a spike by photostimulation of dendrites (Pspike = 0.06 ± 0.03, n = 58 dendritic targets, 8 cells, mean ± sem).

Mapping local functional connectivity in layer 4 barrel cortex

Having established the parameters for single cell 2P photostimulation, we used this technique to map functional excitatory connectivity between stellate cells in layer 4 barrel cortex. We made whole-cell patch-clamp recordings from individual stellate cells within a barrel in slices prepared from mice aged P4–12 and obtained a 2P image of the cell (Figure 2A, B). We then systematically tested for presynaptic cells connected to the recorded cell by stimulating a number of cell somata over multiple trials in a pseudorandom order (Figure 2B, C; Supplemental Experimental Procedures). For most cells stimulated, no evoked response in the postsynaptic (recorded) neuron was observed (Figure 2D). However, for a subset of stimulated cells, EPSCs were evoked in the postsynaptic neuron (Figure 2E). These EPSCs occurred within the expected detection period (Figure 2E, I) and exhibited consistent kinetics (Figure 2F) that were indistinguishable from those of spontaneous EPSCs (sEPSCs) recorded in the same cells (Figures 2G & Fig S4C). Although low in frequency, a

NIH-PA Author Manuscript

NIH-PA Author Manuscript

NIH-PA Author Manuscript

proportion of the synaptic events occurring during the detection period may be sEPSCs. Therefore, to objectively and quantitatively define a cell as connected, the frequency of EPSCs in the detection period must exceed the maximal frequency observed in during equivalent baseline periods in that cell (Supplemental Experimental Procedures). Using this detection criterion for evoked EPSCs, the resultant peri-stimulus time distribution of evoked EPSCs closely matched the distribution of spikes evoked by photostimulation, whereas for unconnected neurons there was no change in event frequency associated with photostimulation (Figure 2I).

We have shown that photostimulation of dendrites is highly unlikely (Figure 1B) but, because dendrites are numerous in the neuropil, we further tested the accuracy of photostimulation in identifying the correct presynaptic neurons. In one set of recordings, presynaptic cells identified as connected by photostimulation were further tested for a connection by making a simultaneous whole-cell patch-clamp recording from the same presynaptic neuron (Figure S3A–E). In all cases tested, the presynaptic cell was found to be connected (n = 4). In a second subset of recordings, we re-tested identified connections by photostimulating with the laser targeted to the other side of the same soma (Figure S3F, G). If the identified cell soma is the cell that is connected, then targeting the laser to the other side of the same soma should also elicit a response in the postsynaptic cell. In all but one case, targeting the opposite side of the same cell soma of detected connected presynaptic neurons elicited postsynaptic responses with a similar frequency. Conversely, in presynaptic cells determined by photostimulation to be unconnected, targeting the other side of the soma never elicited a response. In a final set of control experiments, we explicitly measured if photostimulation of dendrites can ever elicit false positives for connections. To do this, we targeted the laser to regions of the neuropil that lack cell bodies, thereby only uncaging onto dendrites and axons. We replicated the protocol used when targeting somata and measured the number of connections detected. In slices from P9–10 animals, we tested 192 photostimulation locations in neuropil and detected zero connections. This is in contrast to a connectivity rate of 13% detected using the photostimulation of cell somata. Taken together, these three sets of control experiments directly demonstrate that the photostimulation method triggers spiking in single identified cell bodies and not their neighbors or nearby dendrites.

Currents were occasionally evoked by direct photostimulation of dendrites of the recorded cell. These had relatively slow kinetics and were always easily distinguished from EPSCs (Figure S4). Importantly this allows mapping of connectivity close to the recorded cell within the region that contains the postsynaptic dendrites. Thus we confirm criterion number five, the unambiguous detection of evoked synaptic events.

The weak synaptic strength we observe for connections between stellate cells (Figure 2, see also Figure 4A, B) and the small numbers of spikes induced by photostimulation (Figure S2C) makes it very unlikely that activation of a single neuron by photostimulation can elicit action potentials in postsynaptic partners. Indeed, in agreement with others (Lefort et al., 2009; Feldmeyer et al., 1999), we find using current clamp recordings that the unitary connections between stellate cells are never strong enough to evoke action potentials (not shown). Therefore it is unlikely that EPSCs evoked by photostimulation are generated by anything other than monosynaptic input onto the recorded cell, thereby fulfilling criterion number six.

Thus 2P-photostimulation, using the parameters we have defined, can generate maps of connectivity. To generate these functional connectivity maps we reconstructed the soma and dendrites of the postsynaptic recorded neuron using the 2P fluorescence image that was obtained for all recordings. Onto this was mapped the 3-D location of all of the somata that

NIH-PA Author Manuscript

NIH-PA Author Manuscript

NIH-PA Author Manuscript

were targeted by photostimulation and the approximate location of the barrel walls. The strength of the synaptic connection (unitary synaptic strength) was overlaid on this map using a color scale (Figure 2H; see Figure S5 for a second example experiment).

Experience drives an abrupt increase in synaptic connectivity

We constructed connectivity maps to investigate the day-by-day development of the excitatory stellate cell network in individual barrels during the first two postnatal weeks and assessed the role of sensory experience in driving changes to this network (Figure 3A). This is a period when layers 4 and 2/3 of barrel cortex undergo functional maturation that is highly sensitive to sensory experience (Feldman et al., 2005). During the first postnatal week the probability of a connection between two stellate cells (Pconnection) was on average very low (~4 %), demonstrating that little local connectivity exists at this early stage of life. However, at P9 an abrupt 3-fold increase in Pconnection occurred that persisted at least until P12 (Figure 3B). The increase in connectivity emerged very rapidly (over just one day), indicating a period of intense functional synapse formation or potentiation. This statistically significant step up in connectivity prompted us to consider two age groups; young (P4–8, mean connectivity = 0.038) and old (P9–12, mean connectivity = 0.129, Figure 3C). Analysis of the distribution of Pconnection values for individual cells shows that the increase in connectivity is due not only to a general shift in the distribution to larger Pconnection values, but also the emergence of cells that exhibit very high Pconnection values of 0.6– 0.7 (Figure 3C; P4–8 SD = 0.067, P9–12 SD = 0.205). Such high connectivity cells could represent ‘hub’ neurons that are proposed to play an important role in information processing and coordinating network activity (Grinstein and Linsker, 2005; MacLean et al., 2005; Bonifazi et al., 2009). We also observed a transient increase in connectivity at P6, but because of its transient nature it is unclear if this increase is important or whether it is a sampling anomaly in our data set. As a confirmation of this connectivity analysis, we made paired recordings between stellate cells from the two age groups and found similarly low connectivity in young cells (P4–8, 4.4%, 3/68 positive connections) that jumped ~3 fold in the older group (P9–12, 15.6%, 12/75 connections, $p<0.05$).

In interleaved experiments we analyzed whether sensory experience is required for the developmental increase in Pconnection. To deprive experience, all whiskers on the whisker pad contralateral to the analyzed barrel cortex were trimmed daily from birth until the day of the experiment. Importantly neurons in deprived barrels showed no differences in passive membrane properties (data not shown) or in their response to 2P-photostimulation compared to controls (Figure S2). Whisker trimming completely prevented the increase in connectivity at P9 resulting in a low level of connectivity at P9– 12 in deprived barrels similar to that observed in the first postnatal week (Figure 3A, B, C). Thus whisker-driven sensory experience is required for the rapid increase in stellate cell functional connectivity at P9.

Synaptic strength is regulated independently of experience

We analyzed the synaptic properties of the connections detected by photostimulation, calculating three parameters: unitary amplitude (average amplitude of the synaptic response across all trials), success rate (the fraction of presynaptic action potentials producing an EPSC) and potency (amplitude of evoked EPSCs ignoring failures) (see Supplemental Experimental Procedures).

Unitary amplitude of the connections was on average small; however, the distribution showed a long tail of connections with larger amplitudes (Figure 4A). This is consistent with previous work on neocortex, including that from barrel cortex, showing that there is a small proportion of connections that are strong, whereas the majority are weak (Lefort et al., 2009; Feldmeyer et al., 1999; Song et al., 2005). The mean unitary amplitude of the connections

NIH-PA Author Manuscript

NIH-PA Author Manuscript

NIH-PA Author Manuscript

was on average small but did show a trend to a gradual increase in unitary amplitude during development (Figure 4B), which was associated with an increase in the reliability of transmission (success rate; Figure S6A). In contrast, the absolute size of EPSCs remained relatively constant during this developmental period (potency; Figure S6B). In contrast to connectivity, no rapid change in any synaptic properties was observed at any one developmental time point. In whisker-trimmed animals, unitary EPSC amplitude, success rate and potency were very similar to stellate cells in undeprived barrels at the same age (Figure 4B & S6A,B). Thus, unlike functional connectivity, synaptic function between stellate cells appears to change only gradually during development and is regulated independent of sensory experience.

A selective increase in connections between nearby neurons produces a highly recurrent network

An inverse relationship between connectivity probability and distance between neurons has been noted at different scales within the cortex, including local microcircuits (Braitenberg et al., 1998; Holmgren et al., 2003; but see Song et al., 2005; Lefort et al., 2009). To assess this characteristic during development of the layer 4 local circuit, we analyzed the relationship between inter-soma distance and connectivity or synaptic strength. Pconnection at P4–8 exhibited a weak inverse dependence on distance, such that cells closer together had a slightly higher probability of being connected (Figure 3E). Pconnection at P9–12, however, was strongly dependent on distance with ~5 fold increased chance of cells 20 μm apart being connected compared to those 100 μm apart. Thus, even though the axonal and dendritic arbors of the cells are rapidly growing to span larger volumes at this developmental stage (Figures 3A & 6A), the rapid increase in connectivity at P9–12 is due to a preferential increase in connections between close neighbors. In contrast to connectivity, neither unitary amplitude nor success rate showed any consistent relationship with distance for either age group (Figure S6C, D). Thus it appears that the increase in connectivity at P9 is produced by adding synaptic connections between near neighbors that are of similar strength to those already present in the network.

We investigated the implications of the increase in connectivity for the layer 4 stellate cell network using graph theory and Monte Carlo simulations. Connections were assigned to adjacency matrices representing the P4–8 (Figure 5A) and P9–12 (Figure 5B) networks by sampling the experimentally-determined Pconnection distribution (Figure 3D) and distance-Pconnection relationship (Figure 3E; Supplemental Experimental Procedures). The increase in connectivity at P9 drives up the total number of connections within the network as expected (Figure 5C, D). We quantified how recurrent the different networks are (i.e. - how easy is it for a cell's activity to feed back onto itself) by measuring the number of connections that return to the starting cell ('recurrent cycles') for a given path length (number of connections; Figure 5E) (Bullmore and Sporns, 2009). A path length of 2 represents reciprocal connections and we found that the 3-fold increase in mean connectivity at P9 is predicted to cause a 15-fold increase in the number of reciprocal connections between stellate cells. An even larger effect on the number of cycles is predicted for longer path lengths, for example an ~1,000 fold increase for a path length of 5 due to the change in connectivity at P9 (Figure 5E). Thus the 3-fold increase in connectivity between individual stellate cells is predicted to produce a very large increase in the recurrency of the entire network.

We also analyzed the effect of the increase in connectivity on other features of network architecture (Figure 5F, G & Table S1). This analysis shows that the P9–12 network has a short average path length (the average number of connections between any two neurons) and a high degree of clustering (the degree to which neighboring cells are interconnected; Figure 5F), producing a network that has 'small-world' architecture (Bullmore et al., 2009; Watts

NIH-PA Author Manuscript

NIH-PA Author Manuscript

NIH-PA Author Manuscript

and Strogatz, 1998). By comparing the P9–12 network to a randomly-generated network with the same average connectivity but lacking the experimentally-measured connectivity features, we assessed the effects of our experimentally-observed Pconnection distribution and distance-Pconnection relationship on network architecture. We calculated the ratio of the number of short length recurrent loops in the experimental and random networks. More recurrent paths exist in the experimental model despite the same average number of connections (Figure 5G). For example, reciprocal connections are found with a 70% higher incidence compared to the random networks. Thus our analysis indicates that it is the preferential increase in local connectivity that promotes the existence of short recurrent synaptic loops. An unusually high prevalence of local reciprocal connections has also been found in several other studies of neocortical connectivity (Song et al., 2005; Holmgren et al., 2003; Markram et al., 1997; but see Lefort et al., 2009).

The increase in connectivity is associated with spinogenesis in stellate cells

Are there anatomical correlates of the rapid change in functional connectivity at P9? To investigate this question we reconstructed live 2P images of the recorded neurons and analyzed developmental and experience-dependent changes in dendrites and spines (Figure 6A – C). From P4 to P13 there was a progressive increase in dendritic length and complexity that was uniform throughout this developmental period and was insensitive to whisker deprivation (Figure 6D). When spines were analyzed (Figure 6E) we found that during the first postnatal week (P4–P8) stellate cells almost entirely lacked spines. However, beginning at P9 there was a rapid, profound spinogenesis, with a ~70 fold increase in spine number between P8–P9 and a ~250 fold increase from P8 to P13 (Figure 6F). The spinogenesis shows a striking developmental correlation with the increase in functional connectivity between stellate cells observed at P9. However, in marked contrast to the increase in connectivity, the spinogenesis was not prevented by whisker deprivation (Figure 6A–C, E).

Sensory experience controls the number of AMPAR-silent spines

One hypothesis to explain the dissociation in the mechanisms regulating functional connectivity and spinogenesis is that new spines are initially silent (lack postsynaptic AMPARs, but contain NMDA receptors [NMDARs]) (Liao et al., 1995; Isaac et al., 1995; Kerchner and Nicoll, 2008) and that experience-driven activity is necessary to unsilence them to produce functional AMPAR-containing connections (Takahashi et al., 2003). Previous work has shown that the great majority of excitatory input onto stellate cells is onto spines and originates from other stellate cells within layer 4 (Lefort et al., 2009; Schubert et al., 2003; Benshalom and White, 1986). Therefore, most spines are sites of synapses contributing to the intra-barrel network that we have analyzed. To assess the functionality of the newly-emerged spines, we probed stellate cell spine receptor content using brief 2P glutamate uncaging (0.5–1.5 ms) targeted to individual spines (Matsuzaki et al., 2001). At a holding potential of −70 mV the 2P-evoked responses had a very similar time-course and amplitude to sEPSCs recorded in the same cells (Figure S7A, B), indicating that they largely reflect activation of synaptic AMPARs, as previously reported (Smith et al., 2003; Busetto et al., 2008). We compared the AMPAR and NMDAR-mediated currents evoked by uncaging on spines close to the postsynaptic site and at a nearby dendritic location (Figure S7A, Supplemental Experimental Procedures). By calculating the difference between the spine head and dendrite AMPAR response, we estimated the degree of AMPAR enrichment at the spine head.

For spines in undeprived barrels (P9–13) the amount of spine head AMPAR current varied widely with little correlation between AMPAR current amplitude and spine head size (Figure 7A, B). In a subset of spines there was no AMPAR current, thus indicating that these spines lack AMPARs and are ‘silent spines’. In barrels deprived of whisker experience the

NIH-PA Author Manuscript

NIH-PA Author Manuscript

NIH-PA Author Manuscript

average spine AMPAR current was greatly reduced and the fraction of silent spines was doubled, to 80% (Figure 7C,D, 53 spines, 19 slices). Importantly we assayed the same sized spines in both undeprived and deprived barrels (Figure S7C). Interestingly, although there was little correlation between spine head size and AMPAR current for the whole spine population, when non-silent spines were considered alone, a strong positive correlation between spine head size and AMPAR current amplitude was observed (Figure S7D, Pearson's correlation coefficient = 0.484, $p<0.05$)(Matsuzaki et al., 2001). Taken together, our analyses show that deprivation of sensory experience increases the fraction of AMPAR-silent spines during the neonatal circuit maturation.

Synaptic connectivity mediated by NMDA receptors is insensitive to experience

The spine uncaging experiments revealed substantial NMDAR currents (at +40mV) at nearly all spines tested, which may suggest that synaptic connectivity mediated via NMDARs develops independent of experience. To investigate this issue, we tested the effect of whisker trimming on the extent of connectivity mediated by NMDARs using photostimulation of presynaptic cells while recording from the postsynaptic neuron at a holding potential of +40mV. We were able to readily record and identify spontaneous and evoked outward EPSCs of >10pA peak amplitude (Figure 8A and S8A). Compared to those recorded at −60mV, EPSCs were relatively slow rising and decaying (Figure 8B), but were still easily distinguished from currents evoked by direct activation of the postsynaptic dendrites by glutamate uncaging (Figure S4C). Our recording solution composition and the antagonism of $GABA_A$ receptors by MNI-caged glutamate (>95% block of IPSCs at the concentration we use, n=3; Fino et al., 2009) meant that GABAergic currents did not contribute to evoked responses (see Supplemental Experimental Procedures). Similar to connectivity mediated by AMPARs, we constructed maps based on NMDAR connectivity within barrels from P9–12 animals that had been whisker trimmed from birth and from their untrimmed littermates (Figure 8C). In contrast to the reduced connectivity via AMPARs, we found no effect of whisker trimming on synaptic connectivity mediated by NMDARs (Figure 8D). There was also no difference in the size or reliability of evoked EPSCs in control and whisker-trimmed animals (Figure 8E & S8BC). Although there may be some small amplitude NMDA receptor-mediated connections that are below our threshold for detection, the distribution of amplitudes of spontaneous EPSCs showed no differences between control and trimmed experiments (Figure S8A), suggesting that this proportion remained the same in the two conditions. . Taken together with the spine function analysis, our data suggest that NMDA receptor-mediated synaptic connections at dendritic spines develop via experience-independent mechanisms and sensory experience acts to recruit AMPARs to these connections to produce the functional network.

DISCUSSION

Local excitatory connections represent the largest excitatory input onto glutamatergic neocortical neurons and are predicted to play an important role in information processing (Douglas et al., 2004). However, traditionally the properties of these networks have been difficult to study due to their sparse connectivity. Our new 2P glutamate uncaging-based method now provides a relatively high throughput approach to quantitatively study the properties of local circuits. Our approach is considerably faster than traditional methods using simultaneous intracellular recordings and circumvents the significant problems of the previous 2P uncaging techniques (see Supplemental Introduction). By using a relatively long uncaging period, but restricting the uncaging location to a small volume, we achieve single cell spatial resolution. The long uncaging period has a second major advantage, which is that it is easy to distinguish synaptic events and those produced by directly uncaging onto dendrites of the recorded cell based on kinetics. This means that connectivity of nearby

NIH-PA Author Manuscript

NIH-PA Author Manuscript

NIH-PA Author Manuscript

neurons within the dendritic field of the recorded neuron can be measured. Indeed, this feature is critical to understanding connectivity of the layer 4 excitatory network because connectivity is highest for nearby neighbors.

The disadvantage of our 2P uncaging approach is that the timing of spikes evoked by the uncaging is not precise and the number of spikes variable between cells. This feature means that one has to account for the possibility that some of the responses during the 2P uncaging response period are spontaneous EPSCs not evoked from the targeted presynaptic neuron. Although we show that one can objectively determine if 2P uncaging evokes synaptic responses, the rate of spontaneous events defines a success rate threshold for evoked responses below which a connection cannot be unambiguously detected. Thus if there is a high rate of spontaneous synaptic activity in a recorded cell, a proportion of low success rate (unreliable) connections will be missed. Fortunately in layer 4 stellate cells at the ages we have studied, the spontaneous event rate is low.

The role of experience in shaping sensory-evoked responsiveness of the cortex has long been noted (Diamond et al., 1994; Feldman et al., 2005; Hensch, 2005). Also, manipulations of sensory experience can drive pre- and post-synaptic plasticity at various intra-cortical pathways, particularly when they occur early in development (Katz and Shatz, 1996; Allen et al., 2003; Bender et al., 2006; Cheetham et al., 2007; Glazewski and Fox, 1996; Takahashi et al., 2003; Celikel et al., 2004). These data and direct measures of gross intracortical connectivity (Shepherd et al., 2003) suggest that the development of cortical circuitry is likely driven by sensory activity-evoked changes in synaptic connectivity and strength (Feldman, 2009). Here, we have used our 2P photostimulation to measure this process in a defined intracortical microcircuit at the level of individual neurons and reveal the experience-dependent mechanisms driving network formation. Our study reveals a remarkably rapid and specific sensory-driven change in the stellate cell network in layer 4 barrel cortex; a 3-fold increase in functional connectivity occurring in one day at P9 converts the network from a weakly connected state to one predicted to be strongly recurrent. Another striking feature of the maturation of the layer 4 excitatory network is the emergence of dendritic spines concurrent with the connectivity increase at P9; in striking contrast to connectivity, this emergence does not depend on intact sensory experience. A developmental increase in cortical synapse and spine number has been previously noted (White et al., 1997; Lubke et al., 2000; De Felipe et al., 1997) but the relationship between spinogenesis, synaptic function and sensory experience has not been defined. Our findings show that perturbing sensory experience results in the emergence of spines that have NMDARs but lack AMPARs. Interestingly, we found that even apparently silent spines often had mature anatomical characteristics (large head, well-defined neck). This highlights the difficulty in making anatomically-based predictions of synapse and circuit function. Our uncaging experiments do not confirm that newly-formed spines targeted for uncaging have functional presynaptic partners, but electron microscopic studies in barrel cortex of developing mice have found that almost all spines are associated with a presynaptic bouton (Micheva and Beaulieu, 1996; De Felipe et al., 1997; White et al., 1997). In line with this, we found that synaptic connectivity via NMDARs, like the emergence of spines, was undiminished by sensory perturbation. These experiments suggest that NMDAR-only synapses at anatomically mature spines emerge via mechanisms intrinsic to the cortex. This network provides the template upon which experience-dependent activity can shape functional connectivity by recruiting AMPARs to the appropriate spines and thereby unsilencing them (Liao et al., 1995; Isaac et al., 1995; Takahashi et al., 2003). Direct comparison of rates of AMPAR and NMDAR connectivity are difficult because of their differing recording conditions in our experiments. It will be interesting in the future to directly address whether an excessive NMDAR connectivity is established and pruned back

NIH-PA Author Manuscript

NIH-PA Author Manuscript

NIH-PA Author Manuscript

or whether the physical connectivity is matched by experience-dependent functional synaptic and network maturation.

Theoretical studies suggest that mature neocortical networks exhibit a small-world network architecture that facilitates information processing by enabling extraction of sensory stimulus from a noisy input (Buonomano et al., 2009; Haeusler et al., 2009; Douglas and Martin, 2007; Humphries and Gurney, 2008). Our work suggests that the experience-dependent addition of new functional connections between nearby neighbors on top of an existing low level of connectivity independent of distance, produces small-world architecture. Further we show that this process is predicted to produce a highly recurrent yet sparsely connected excitatory network of the type that is typically observed in neocortex. It has been shown that connected neurons in the visual cortex are more likely to form specific microcircuits with common input neurons (Yoshimura et al., 2005) and the selective establishment of near-neighbor and highly reciprocal connectivity is at the heart of the network properties generated by our model. It will be very interesting to determine whether there are small, local clusters of synaptically-connected neurons that share common thalamocortical input and whether the activity of such inputs is instructive in the establishment of the local intracortical connectivity. However, because connectivity is sparse, it is likely that large numbers of multi-electrode recordings to test reciprocal connectivity will be required for this task. The timing of the layer 4 barrel circuit maturation closely precedes the onset of sensory-evoked spiking and opening of the critical period for receptive field plasticity in layer 2/3 (Stern et al., 2001). Therefore, changes in layer 4 spike rate or timing driven by emergence of recurrent connectivity within the barrel may be the prerequisite for development of downstream sensory-evoked cortical activity.

EXPERIMENTAL PROCEDURES

Whole cell patch clamp was used to record from individual or pairs of excitatory neurons located in barrel structures of acutely-prepared somatosensory cortex slices from neonatal (P4–P13) mouse pups. Stimulation of putative presynaptic neurons within the same barrel was achieved by on-demand 2-photon uncaging of MNI-glutmate targeted to a spot adjacent to the cell soma, guided by high contrast, transmitted light images. Recording, post-acquistion detection and statistical anaylsis of EPSCs was used to define the presence and the properties of synaptic connections. Recorded cells were routinely filled and imaged using 2-photon microscopy to allow anatomical reconstructions of dendritic arbors. Characterisitics of connectivity were analyzed day-by-day and used to generate a network model using Graph Theory, allowing analysis of changes in network interconnectivity. For measurement of dendritic spine glutamate receptor content, brief (~1ms) uncaging targeted to the heads of single spines was used to evoke EPSCs. Full details of experiments and analysis are found in Supplemental Experimental Procedures.

Supplementary Material

Refer to Web version on PubMed Central for supplementary material.

Acknowledgments

We thank members of the Isaac, Diamond and McBain labs for helpful discussions during this study and to Dietmar Plenz for advice on network topology and graph theoretical analysis. We thank Dr. Ramesh Chittajallu and Dr. Sarah Caddick for contributing to the paired recording connectivity data set. Supported by the NINDS Intramural program.

NIH-PA Author Manuscript

NIH-PA Author Manuscript

NIH-PA Author Manuscript

REFERENCES

Allen CB, Celikel T, Feldman DE. Long-term depression induced by sensory deprivation during cortical map plasticity in vivo. Nat Neurosci. 2003; 6:291–299. [PubMed: 12577061]

Bender KJ, Allen CB, Bender VA, Feldman DE. Synaptic basis for whisker deprivation-induced synaptic depression in rat somatosensory cortex. J. Neurosci. 2006; 26:4155–4165. [PubMed: 16624936]

Benshalom G, White EL. Quantification of thalamocortical synapses with spiny stellate neurons in layer IV of mouse somatosensory cortex. J Comp Neurol. 1986; 253:303–314. [PubMed: 3793995]

Bonifazi P, Goldin M, Picardo MA, Jorquera I, Cattani A, Bianconi G, Represa A, Ben-Ari Y, Cossart R. GABAergic hub neurons orchestrate synchrony in developing hippocampal networks. Science. 2009; 326:1419–1424. [PubMed: 19965761]

Braitenberg, V.; Schüz, A. Cortex: Statistics and Geometry of Neuronal Connectivity. 2nd ed. Springer; 1998.

Bruno RM, Sakmann B. Cortex is driven by weak but synchronously active thalamocortical synapses. Science. 2006; 312:1622–1627. [PubMed: 16778049]

Bullmore E, Sporns O. Complex brain networks: graph theoretical analysis of structural and functional systems. Nat. Rev. Neurosci. 2009; 10:186–198. [PubMed: 19190637]

Buonomano DV, Maass W. State-dependent computations: spatiotemporal processing in cortical networks. Nat. Rev. Neurosci. 2009; 10:113–125. [PubMed: 19145235]

Busetto G, Higley MJ, Sabatini BL. Developmental presence and disappearance of postsynaptically silent synapses on dendritic spines of rat layer 2/3 pyramidal neurons. J. Physiol. (Lond.). 2008; 586:1519–1527. [PubMed: 18202095]

Celikel T, Szostak VA, Feldman DE. Modulation of spike timing by sensory deprivation during induction of cortical map plasticity. Nat Neurosci. 2004; 7:534–541. [PubMed: 15064767]

Cheetham CEJ, Hammond MSL, Edwards CEJ, Finnerty GT. Sensory experience alters cortical connectivity and synaptic function site specifically. J Neurosci. 2007; 27:3456–3465. [PubMed: 17392462]

Dantzker JL, Callaway EM. Laminar sources of synaptic input to cortical inhibitory interneurons and pyramidal neurons. Nat Neurosci. 2000; 3:701–707. [PubMed: 10862703]

De Felipe J, Marco P, Fairén A, Jones EG. Inhibitory synaptogenesis in mouse somatosensory cortex. Cereb. Cortex. 1997; 7:619–634. [PubMed: 9373018]

Diamond ME, Huang W, Ebner FF. Laminar comparison of somatosensory cortical plasticity. Science. 1994; 265:1885–1888. [PubMed: 8091215]

Douglas RJ, Koch C, Mahowald M, Martin KA, Suarez HH. Recurrent excitation in neocortical circuits. Science. 1995; 269:981–985. [PubMed: 7638624]

Douglas RJ, Martin KA. Neuronal circuits of the neocortex. Annu Rev Neurosci. 2004; 27:419–451. [PubMed: 15217339]

Douglas RJ, Martin KA. Recurrent neuronal circuits in the neocortex. Curr Biol. 2007; 17:R496–R500. [PubMed: 17610826]

Feldman DE, Brecht M. Map plasticity in somatosensory cortex. Science. 2005; 310:810–815. [PubMed: 16272113]

Feldman DE. Synaptic mechanisms for plasticity in neocortex. Annu. Rev. Neurosci. 2009; 32:33–55. [PubMed: 19400721]

Feldmeyer D, Egger V, Lubke J, Sakmann B. Reliable synaptic connections between pairs of excitatory layer 4 neurones within a single 'barrel' of developing rat somatosensory cortex. J Physiol. 1999; 521(Pt. 1):169–190. [PubMed: 10562343]

Fino E, Araya R, Peterka DS, Salierno M, Etchenique R, Yuste R. RuBi-Glutamate: Two-Photon and Visible-Light Photoactivation of Neurons and Dendritic spines. Front Neural Circuits. 2009; 3:2. [PubMed: 19506708]

Glazewski S, Fox K. Time course of experience-dependent synaptic potentiation and depression in barrel cortex of adolescent rats. J Neurophysiol. 1996; 75:1714–1729. [PubMed: 8727408]

NIH-PA Author Manuscript

NIH-PA Author Manuscript

NIH-PA Author Manuscript

Grinstein G, Linsker R. Synchronous neural activity in scale-free network models versus random network models. Proc. Natl. Acad. Sci. U.S.A. 2005; 102:9948–9953. [PubMed: 15998732]

Haeusler S, Schuch K, Maass W. Motif distribution, dynamical properties, and computational performance of two data-based cortical microcircuit templates. J. Physiol. Paris. 2009; 103:73–87. [PubMed: 19500669]

Hensch TK. Critical period plasticity in local cortical circuits. Nat. Rev. Neurosci. 2005; 6:877–888. [PubMed: 16261181]

Holmgren C, Harkany T, Svennenfors B, Zilberter Y. Pyramidal cell communication within local networks in layer 2/3 of rat neocortex. J. Physiol. (Lond.). 2003; 551:139–153. [PubMed: 12813147]

Humphries MD, Gurney K. Network 'small-world-ness': a quantitative method for determining canonical network equivalence. PLoS ONE. 2008; 3:e0002051. [PubMed: 18446219]

Isaac JT, Nicoll RA, Malenka RC. Evidence for silent synapses: implications for the expression of LTP. Neuron. 1995; 15:427–434. [PubMed: 7646894]

Katz LC, Shatz CJ. Synaptic activity and the construction of cortical circuits. Science. 1996; 274:1133–1138. [PubMed: 8895456]

Kerchner GA, Nicoll RA. Silent synapses and the emergence of a postsynaptic mechanism for LTP. Nat Rev Neurosci. 2008; 9:813–825. [PubMed: 18854855]

Lefort S, Tomm C, Floyd Sarria J, Petersen CCH. The excitatory neuronal network of the C2 barrel column in mouse primary somatosensory cortex. Neuron. 2009; 61:301–316. [PubMed: 19186171]

Liao D, Hessler NA, Malinow R. Activation of postsynaptically silent synapses during pairing-induced LTP in CA1 region of hippocampal slice. Nature. 1995; 375:400–404. [PubMed: 7760933]

Lubke J, Egger V, Sakmann B, Feldmeyer D. Columnar organization of dendrites and axons of single and synaptically coupled excitatory spiny neurons in layer 4 of the rat barrel cortex. J Neurosci. 2000; 20:5300–5311. [PubMed: 10884314]

MacLean JN, Watson BO, Aaron GB, Yuste R. Internal dynamics determine the cortical response to thalamic stimulation. Neuron. 2005; 48:811–823. [PubMed: 16337918]

Markram H, Lübke J, Frotscher M, Roth A, Sakmann B. Physiology and anatomy of synaptic connections between thick tufted pyramidal neurones in the developing rat neocortex. J Physiol. 1997; 500(Pt 2):409–440. [PubMed: 9147328]

Matsuzaki M, Ellis-Davies GC, Nemoto T, Miyashita Y, Iino M, Kasai H. Dendritic spine geometry is critical for AMPA receptor expression in hippocampal CA1 pyramidal neurons. Nat Neurosci. 2001; 4:1086–1092. [PubMed: 11687814]

Matsuzaki M, Ellis-Davies GCR, Kasai H. Three-dimensional mapping of unitary synaptic connections by two-photon macro photolysis of caged glutamate. J Neurophysiol. 2008; 99:1535–1544. [PubMed: 18216227]

Nikolenko V, Poskanzer KE, Yuste R. Two-photon photostimulation and imaging of neural circuits. Nat Methods. 2007; 4:943–950. [PubMed: 17965719]

Petersen CC. The barrel cortex--integrating molecular, cellular and systems physiology. Pflugers Arch. 2003; 447:126–134. [PubMed: 14504929]

Petreanu L, Huber D, Sobczyk A, Svoboda K. Channelrhodopsin-2-assisted circuit mapping of long-range callosal projections. Nat. Neurosci. 2007; 10:663–668. [PubMed: 17435752]

Rigas P, Castro-Alamancos MA. Impact of persistent cortical activity (up States) on intracortical and thalamocortical synaptic inputs. J. Neurophysiol. 2009; 102:119–131. [PubMed: 19403750]

Schubert D, Kotter R, Zilles K, Luhmann HJ, Staiger JF. Cell type-specific circuits of cortical layer IV spiny neurons. J Neurosci. 2003; 23:2961–2970. [PubMed: 12684483]

Shepherd GM, Pologruto TA, Svoboda K. Circuit analysis of experience-dependent plasticity in the developing rat barrel cortex. Neuron. 2003; 38:277–289. [PubMed: 12718861]

Smith MA, Ellis-Davies GCR, Magee JC. Mechanism of the distance-dependent scaling of Schaffer collateral synapses in rat CA1 pyramidal neurons. J. Physiol. (Lond.). 2003; 548:245–258. [PubMed: 12598591]

Song S, Sjostrom PJ, Reigl M, Nelson S, Chklovskii DB. Highly nonrandom features of synaptic connectivity in local cortical circuits. PLoS Biol. 2005; 3:e68. [PubMed: 15737062]

NIH-PA Author Manuscript

NIH-PA Author Manuscript

NIH-PA Author Manuscript

Stern EA, Maravall M, Svoboda K. Rapid development and plasticity of layer 2/3 maps in rat barrel cortex in vivo. Neuron. 2001; 31:305–315. [PubMed: 11502260]

Takahashi T, Svoboda K, Malinow R. Experience strengthening transmission by driving AMPA receptors into synapses. Science. 2003; 299:1585–1588. [PubMed: 12624270]

Thomson AM, West DC, Wang Y, Bannister AP. Synaptic connections and small circuits involving excitatory and inhibitory neurons in layers 2–5 of adult rat and cat neocortex: triple intracellular recordings and biocytin labelling in vitro. Cereb. Cortex. 2002; 12:936–953. [PubMed: 12183393]

Watts DJ, Strogatz SH. Collective dynamics of 'small-world' networks. Nature. 1998; 393:440–442. [PubMed: 9623998]

White EL, Weinfeld L, Lev DL. A survey of morphogenesis during the early postnatal period in PMBSF barrels of mouse SmI cortex with emphasis on barrel D4. Somatosens Mot Res. 1997; 14:34–55. [PubMed: 9241727]

White EL. Reflections on the specificity of synaptic connections. Brain Res Rev. 2007; 55:422–429. [PubMed: 17258321]

Yoshimura Y, Dantzker JL, Callaway EM. Excitatory cortical neurons form fine-scale functional networks. Nature. 2005; 433:868–873. [PubMed: 15729343]

NIH-PA Author Manuscript
NIH-PA Author Manuscript
NIH-PA Author Manuscript

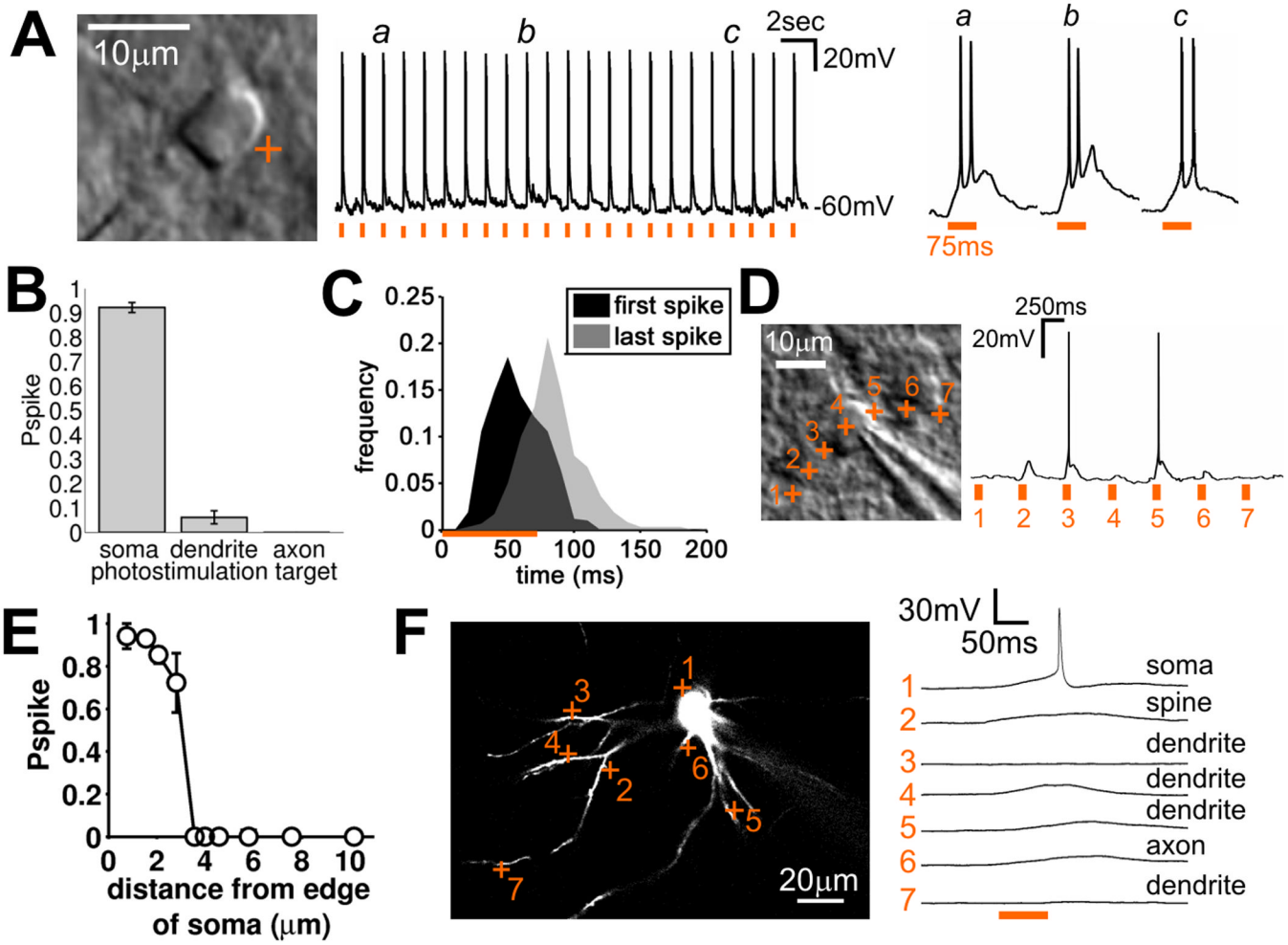

Figure 1. Two photon glutamate uncaging reliably activates neurons with single cell resolution

(A) Dodt gradient contrast image of a recorded cell with photostimulation target indicated (left), response of this neuron to repeated photostimulation (center) and responses to photostimulation for the three indicated examples at higher time resolution (right; orange bars indicate photostimulation). (B) Probability of evoking an action potential by photostimulation targeting different neuronal structures (Pspike = 0.922, n = 70 cells for soma; 0.062, n = 58 locations from 8 cells for dendrite; 0, n = 14 locations from 8 cells for axon, mean ± 95% confidence limits). (C) Frequency histogram of latency to first action potential (black) and last action potential (gray) evoked by photostimulation (577 trials from 70 cells). (D) Dodt gradient contrast image of recorded cell with photostimulation targets at varying distances from the soma indicated (left) and the responses to the photostimulation evoked at those targets (right). (E) Probability of evoking an action potential vs. distance of photostimulation from the edge of the soma (data for all 3 spatial dimensions pooled; 97 locations from 10 cells). (F) 2PLSM image of recorded stellate cell (single z-plane) with photostimulation targets (left) and responses to photostimulation (right).

NIH-PA Author Manuscript
NIH-PA Author Manuscript
NIH-PA Author Manuscript

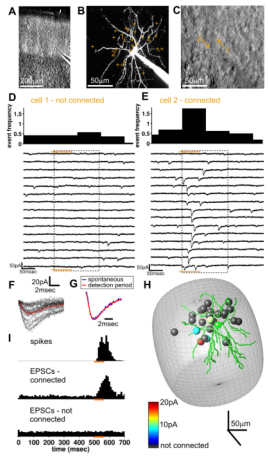

Figure 2. Mapping of synaptic connections using 2P photostimulation

(A) Dodt contrast image of barrel cortex slice. (B) 2P image of recorded cell (maximum projection) with all photostimulation targets indicated (corresponding to individual neuronal somata distributed in 3-D and targeted using Dodt contrast image). (C) Dodt contrast image (single focal plane) with two of the targets from b indicated. (D&E) Responses in the recorded cell to 15 trials for photostimulation of the two putative presynaptic neurons indicated in B & C (orange bar is photostimulation, dashed box is the detection period [defined in Figure 1C]). The binned frequency histogram for detected EPSCs is shown above the traces. Cell 1, shown in D, is not connected but for cell 2, in E, the appearance of EPSCs in the detection period indicates a synaptic connection to the recorded cell. (F) EPSCs from the detection period during photostimulation of presynaptic cell 2 (in E), aligned and superimposed (red is the average). (G) Scaled mean EPSCs from the detection period and mean sEPSC from same celld indicate that the kinetics of spontaneous and evoked EPSCs are indistinguishable. (H) 3-D map of connectivity for the recorded cell. Green is the reconstruction of the postsynaptic cell soma and dendrites. Other spheres represent putative presynaptic neurons tested using photostimulation with strength of connection color coded (4 were connected; slice from P12 animal). Cells are shown at their locations within the barrel (gray structure - estimated from the Dodt contrast image). (I) Time histogram showing action potential latency (top; same data as in Figure 1F) and EPSC event frequency before during and after photostimulation for all connections tested divided into connected (middle; 60 connections tested from 60 recordings) and unconnected (bottom; 983 connections tested from 60 recordings) cells.

NIH-PA Author Manuscript
NIH-PA Author Manuscript
NIH-PA Author Manuscript

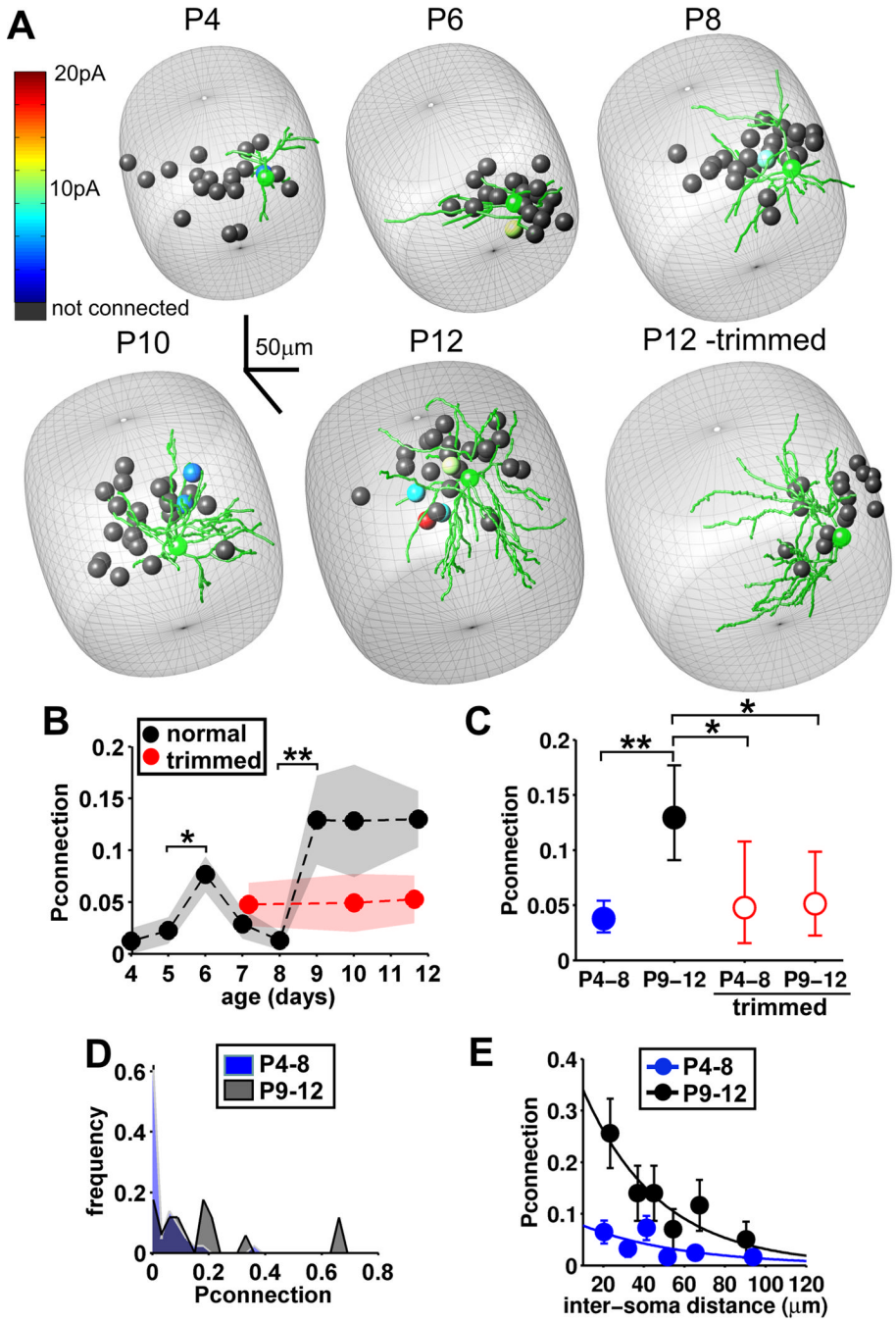

Figure 3. Sensory experience drives an abrupt increase at P9 in stellate cell connectivity

(A) 3-dimensional maps of connectivity for the recorded cells from representative experiments throughout early development and from a deprived barrel at P12. Green is the reconstruction of the postsynaptic cell soma and dendrites. Other spheres represent putative presynaptic neurons tested using photostimulation with strength of connection color coded (4 were connected; slice from P12 animal). Cells are shown at their locations within the barrel (gray structure - estimated from the Dodt contrast image). (B) Connection probability (Pconnection, mean ±sem) at different ages in slices from control (black, normal whisker experience) and whisker-trimmed (red) animals (Control, n = P4, 1/81, 7; P5, 3/133, 10; P6, 18/235, 12; P7, 4/139,7; P8, 2/155,7; P9, 8/62, 5; P10, 5/39, 3; P11, 8/42, 4; P12, 12/112, 5

NIH-PA Author Manuscript

NIH-PA Author Manuscript

NIH-PA Author Manuscript

(age, connectivity, slices). Trimmed, n = P7–8, 5/105, 4; P10, 3/61,3; P11–12, 5/95, 8). (C) Pconnection data pooled as indicated (mean ± 95% confidence limits, P4–8: n = 28/743 connections tested, P9–13: n= 33/255, P4–8 trimmed: n=5/105, P9–12 trimmed: n = 8/156; statistics: Chi-squared test). (D) Frequency histogram of Pconnection for individual cells from P4–8 (blue, n=43) and P9–13 (black, n=17) control animals. (E) Mean Pconnection at different distances (binned) grouped into P4–8 and P9–12 (mean ± sem, P4–8, r^2=0.483, p=0.024; P9–12 r^2=0.842, p=0.010; single exponential fits, Spearman rank correlation).

NIH-PA Author Manuscript

NIH-PA Author Manuscript

NIH-PA Author Manuscript

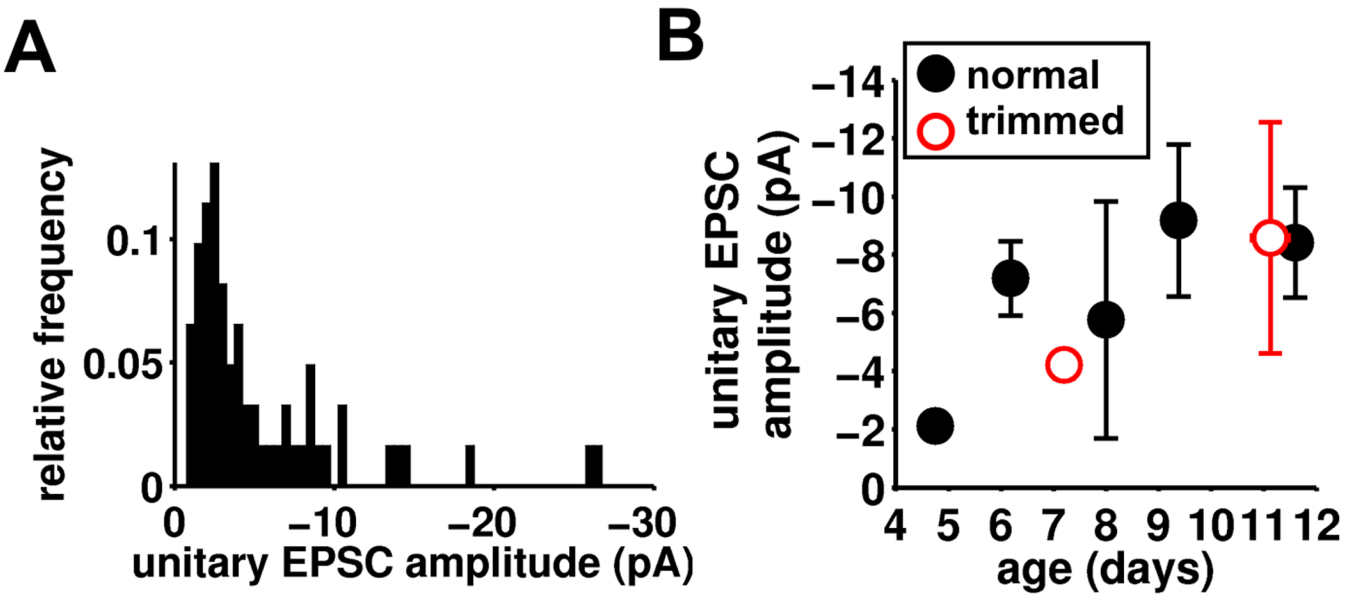

Figure 4. Synaptic properties of the developing stellate cell connections

(A) Frequency histogram of unitary EPSC amplitude for all detected connections (normal whisker experience; n=60). (B) Binned ages vs unitary EPSC amplitude for control (black, n=60) and trimmed (red, n=13) animals.

NIH-PA Author Manuscript
NIH-PA Author Manuscript
NIH-PA Author Manuscript

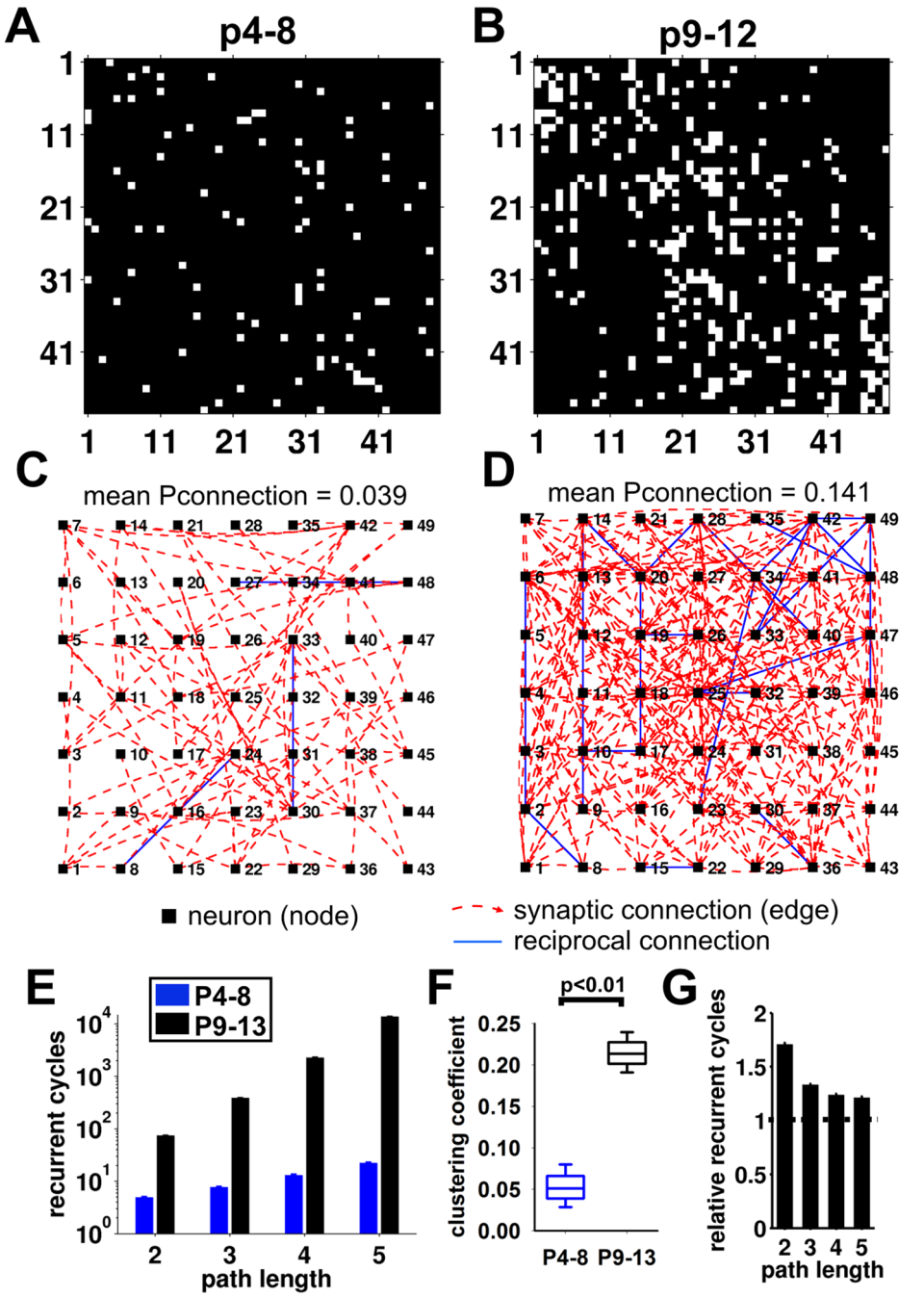

Figure 5. The developmental increase in connectivity is predicted to produce a highly recurrent local circuit

(A&B) Example adjacency matrices for test (using the experimentally determined Pconnection-distance relationship) and matched random (same mean Pconnection but a random Pconnection-distance relationship) networks for (A) P4–8 and (B) P9–12. White pixels represent connected cells, black is not connected. (C&D) Network connection graphs for the adjacency matrices in A & B, respectively. Each node represents the spatial position of a neuron and synaptic connections are shown as dashed red lines (unidirectional – clockwise curve if the cell is presynaptic, anti-clockwise curve if the cell is postsynaptic) or blue (bidirectional – reciprocal). (E) Total number of recurrent cycles for path lengths from

NIH-PA Author Manuscript

NIH-PA Author Manuscript

NIH-PA Author Manuscript

2–5 in modeled networks generated from P4–8 and P9–12 experimental data (for each path length, $p<0.001$, P4–8 vs P9–12). (F) Box plot showing clustering coefficient from modeled P4–8 and P9–13 networks (median ± 95% confidence limits, box shows 25/75 percentiles). (G) Ratio of the number of recurrent cycles of path lengths 2–5 between experimental and matched random networks for P9–12 (mean ± sem).

NIH-PA Author Manuscript

NIH-PA Author Manuscript

NIH-PA Author Manuscript

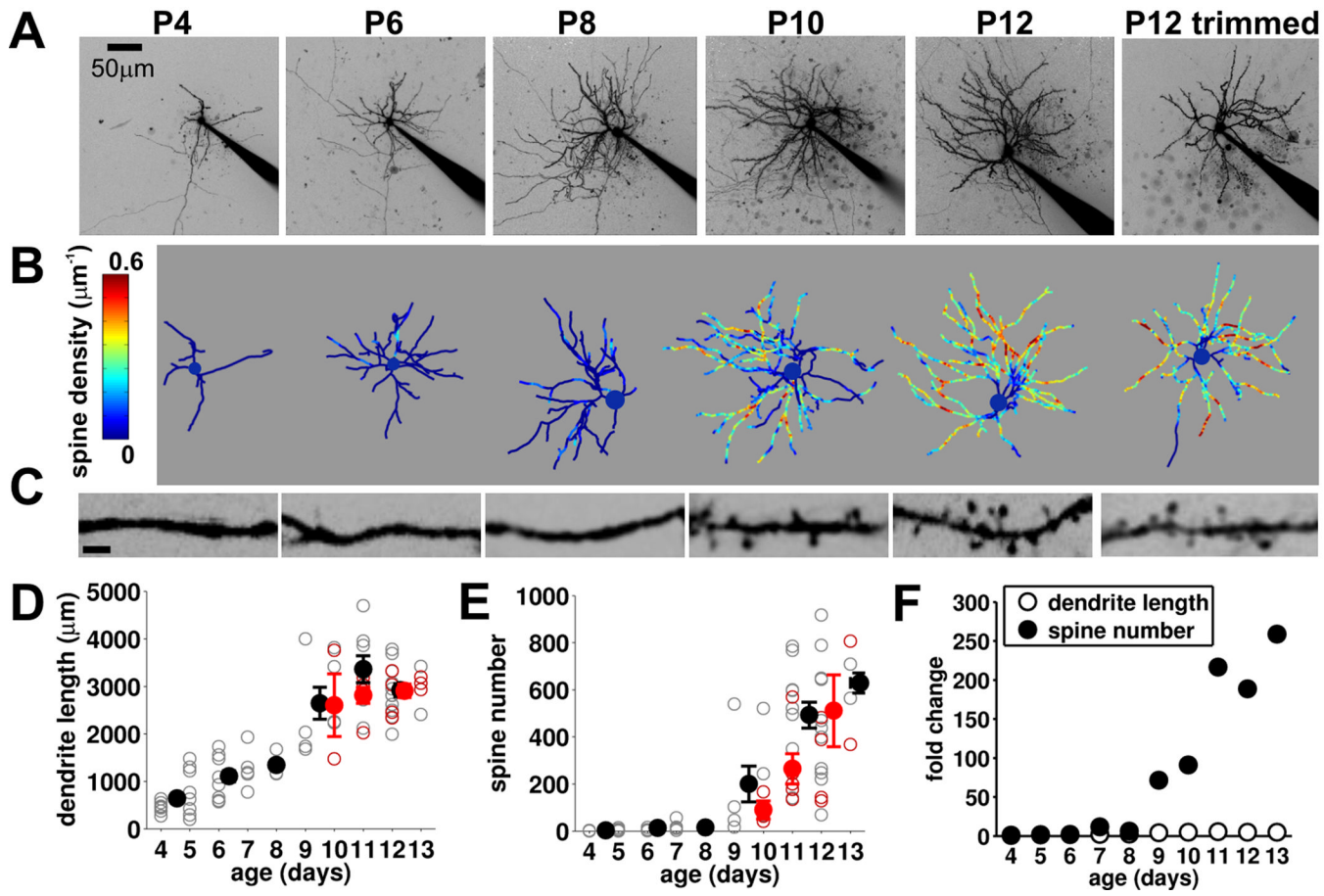

Figure 6. Spinogenesis starting at P9 that is independent of experience

(A) 2P images (maximum projection, inverted contrast for display) of recorded stellate cells at ages indicated (electrode in situ). (B) Reconstructions of soma and dendrites for the same cells with spine density (color coded) superimposed. (C) High power images of representative sections of dendrites from same cells (scale bar, 2 μm). (D) Total dendritic length and (E) spine number vs. age for control (open gray, individual neurons; filled black, mean, n=65) and whisker trimmed (open red, individual neurons; filled red, mean, n=16). (F) Mean data (for control animals) expressed as fold change relative to P4–5 mean value for dendritic length and spine number.

NIH-PA Author Manuscript

NIH-PA Author Manuscript

NIH-PA Author Manuscript

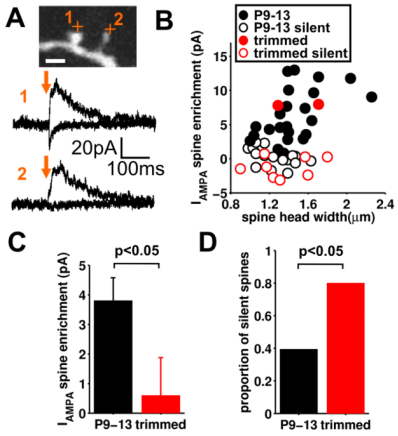

Figure 7. Deprivation of sensory experience results in silencing of spines

(A) Example spine glutamate uncaging experiment showing neighboring AMPA receptor functional and AMPA receptor silent spine on a section of dendrite from a stellate cell (from an undeprived barrel). (B) Spine AMPA receptor current enrichment vs. spine head width for control (undeprived; black) and deprived (red). Open circles are those spines determined to be silent. (C) Pooled data for spine AMPA receptor current enrichment for control (undeprived; black, n=43) and deprived (red, n=10) (mean±sem). (D) The proportion of silent spines in control (undeprived, black) and deprived (red).

NIH-PA Author Manuscript

NIH-PA Author Manuscript

NIH-PA Author Manuscript

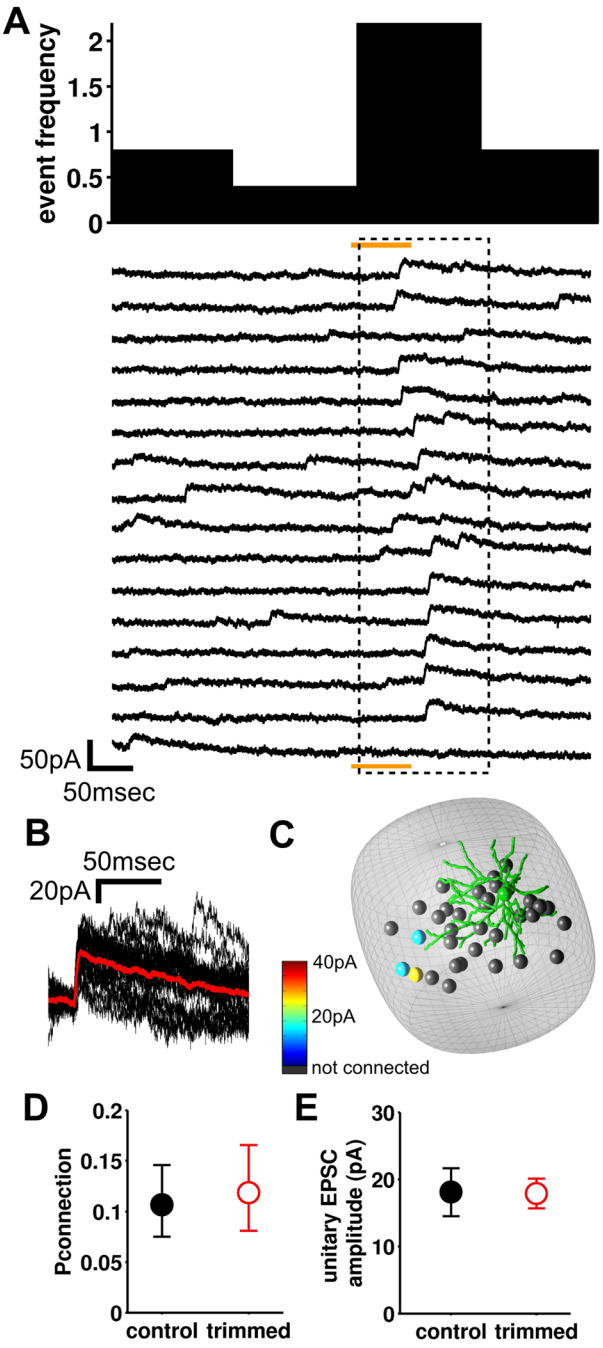

Figure 8. Synaptic connectivity via NMDARs in unchanged by perturbation of sensory experience

(A) Responses in a recorded cell voltage clamped at +40mV during consecutive photostimulation trials of a putative presynaptic neuron (orange bar is photostimulation, dashed box is the detection period). The binned frequency histogram for detected EPSCs is shown above the traces. Note the appearance of slowly-decaying outward NMDAR EPSCs in the detection period indicates a synaptic connection to the recorded cell. (B) EPSCs from the detection period, aligned and superimposed (red is the average). (C) 3-D map of connectivity for the recorded cell. (D) Average probability of connection from P9–12 control and trimmed animals (mean ± 95% confidence limits, control, n= 34/319, 11, 7;

trimmed: n=29/245, 13, 7 (connected/tested cells, recorded cells, animals); Chis-quared test, p=0.76). (E) Mean unitary EPSC amplitude of connections in control and trimmed animals (mean±sem, control, n=34, trimmed, n=29).

NIH-PA Author Manuscript
NIH-PA Author Manuscript
NIH-PA Author Manuscript